Investigation of aeroacoustics and flow dynamics of a NACA 0015 airfoil with a Gurney flap using TR-PIV

Shah, J.; Sciacchitano, Andrea; Pröbsting, Stefan

Publication date
2016

Document Version
Final published version

Published in
Proceedings of the 18th International Symposium on the Application of Laser and Imaging Techniques to Fluid Mechanics

18TH LISBON 2016
INTERNATIONAL SYMPOSIUM
ON APPLICATIONS OF LASER AND IMAGING TECHNIQUES TO FLUID MECHANICS
FROM 4 TO 7 OF JULY

PROCEEDINGS

OF THE

18th INTERNATIONAL

SYMPOSIUM ON

APPLICATION OF

LASER AND IMAGING

TECHNIQUES TO

FLUID MECHANICS

Investigation of aeroacoustics and flow dynamics of a NACA 0015 airfoil with a Gurney flap using TR-PIV

Jiggar Shah[1*], Andrea Sciacchitano[2], and Stefan Pröbsting[2]

1: LaVision GmbH, Göttingen, Germany
2: Faculty of Aerospace Engineering, Delft University of Technology, Delft, The Netherlands
*correspondent author: JShah@lavision.de

ABSTRACT

The present study employs simultaneous planar TR-PIV and microphone measurements to obtain the flow dynamics and aeroacoustic causality correlation associated with a Gurney flap of various sizes in case of low Mach and high Reynolds number flows. The objectives are to investigate the secondary shedding mode for the case of a turbulent boundary layer and to understand the mechanism of noise generation by identifying structures that are highly correlated with far field pressure fluctuations. The instantaneous velocity and vorticity fields show the flapping motion of the wake and the coherent vortex shedding process. The tonal peaks are clearly audible and correspond to the vortex shedding frequency. The PSD of the flow fluctuations and acoustic spectra did not indicate a secondary mode of shedding in case of turbulent boundary layer. The Strouhal numbers of the vortex shedding are found to be close to that of a bluff body in a flow. Causality correlation between pressure fluctuations in the far-field and the near field fluctuations indicates that the vertical velocity in the wake of the model is highly correlated with the far-field pressure fluctuations. This study provides an example of the potential of the causality correlation technique in identifying flow structures/regions highly correlated with noise in case of complex high-lift devices, making it possible to design flaps with lower acoustic emissions.

1. Introduction

For decades, aircraft noise has been subject of research due to the growing number of airports and its effect on surrounding communities (ICAO, 2013). Today, the noise generated by high-lift devices has become comparable to that of turbofan engines (Dobrzynski, 2010). A high-lift device, present on almost any aircraft, is the trailing-edge flap, which exists in a variety of geometries and complexities. One comparatively simple type of flap, which is also found on racing cars (Liebeck, 1978), is the Gurney flap (Figure 1) with a single element oriented at approximately 90° with respect to the airfoil's chord. It may also be considered as a simplified geometry for more complex high-lift devices.

Wang *et al.* (2008) provided a comprehensive summary of past research on the flow structure and on the lift incrementing mechanism of Gurney flaps. Upstream of the flap, the flow separates and forms an upstream recirculation region, similar to a cavity. Downstream of the flap and in the wake of the airfoil, a second recirculation region forms, bounded by the two shear layers originating from the suction and pressure sides (Figure 1) (Liebeck (1978), Jang *et*

al.(1998)). The instantaneous flow field shows a coherent vortex shedding with coherent vortical structures with alternating positive and negative vorticity (Jeffery *et al.* (2000)). Interestingly, Troolin *et al.* (2006) suggested a second mode of shedding apart from this first mode, which they demonstrated by time resolved-particle image velocimetry (TR-PIV) measurements in the case of an un-tripped boundary layer. Moreover, the additional lift produced by a Gurney flap was attributed to this second shedding mode. The existence of this secondary mode of shedding in the flow around a Gurney flap is yet to be investigated for the relevant case of a developed turbulent boundary layer upstream of the trailing edge.

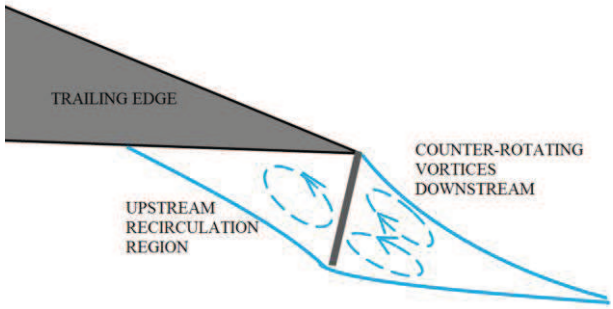

Fig 1: Mean flow field in the presence of a Gurney flap (reproduced from Liebeck, 1978)

To investigate the relation between the unsteady flow field and the sound perceived by a receiver, a technique for combining flow field diagnostics and acoustic measurements has been proposed by several researchers in the past (Siddon (1973), Lee *et al.* (1972), Panda *et al.* (2005), Henning *et al.* (2008)). One approach, that received ample attention in the past, is called causality correlation and requires simultaneous measurements of a source field quantity $\emptyset(\boldsymbol{y}, t)$ and the acoustic pressure $p'(\mathbf{x}, t)$ in the far field. With τ being the time shift between the two signals, the correlation coefficient normalised by the root-mean-square values of $\emptyset$ and p' is defined as (Henning *et al.*, 2008):

$$R_{\emptyset,p'}(\boldsymbol{x}, \boldsymbol{y}, \tau) = \frac{\langle \emptyset(\mathbf{y},t)\, p'(\mathbf{x}, t+\tau) \rangle}{\sigma_{\emptyset}(\boldsymbol{y})\, \sigma_{p'}(\boldsymbol{x})} \quad (1)$$

Examples for the near-field quantity $\emptyset(\boldsymbol{y}, t)$ are the velocity fluctuations $\boldsymbol{v}'$, or the vorticity fluctuations $\boldsymbol{\omega}'$, but also quantities motivated by acoustic analogies, such as the Lamb-vector, have been considered (Henning *et al.*, 2008). The causality correlation technique, using non-intrusive whole field PIV measurements, has previously been applied for the case of coherent vortex shedding behind a cylinder (Henning *et al.*, 2008), vortex-structure interaction on a rod-airfoil configuration (Henning *et al.*, 2010), a cold jet (Henning *et al.*, 2010), and slat

aeroacoustics (Henning *et al.*, 2012). It allows to discriminate between different areas of the source region and, therefore, to separate noise sources associated with the upstream cavity mode or with the wake mode on a Gurney flap. Pröbsting *et al.* (2016) have used causality correlation of the velocity field with the near field surface pressure to the convection velocity associated with coherent vortex shedding behind a semi-blunt trailing edge.

Therefore, the present study employs planar TR-PIV to obtain, at a high spatial and temporal resolution, the flow dynamics and aeroacoustic causality correlation associated with a Gurney flap of various sizes in case of low Mach and high Reynolds number flows. The objectives are to investigate the secondary shedding mode for the case of a turbulent boundary layer and to understand the mechanism of noise generation by identifying structures that are highly correlated with far field pressure fluctuations.

2. Experimental Set-up

The experiments are carried out at the vertical wind tunnel facility (V-tunnel) of the Aerodynamic Laboratories of TU Delft. The V-tunnel is an open-section low- turbulence facility with a circular cross-section of diameter 60 cm, operating in the velocity range between 5 and 45 m/s with free stream turbulence intensity below 1%. For the present study, a circular-to-square adaptor is used at the exit of the tunnel to achieve a square test section of 40×40 cm^2. Similar to work of Troolin *et al.* (2006) Gurney flaps are mounted on a NACA 0015 (Figure 2). The airfoil model has a chord of 20 cm and a span of 40 cm. Three different Gurney flap heights are considered, namely 2%, 4% and 6% of the airfoil chord respectively (as in Troolin *et al*, 2006). The models are tested at 4° and 8° angle of attack at freestream velocity of 20 m/s (Re_c = 270,000) and 30 m/s (Re_c = 400,000). To ensure a fully turbulent boundary layer, roughness elements consisting of carborundum grains of nominal height 0.841 mm are used to trip the boundary layer at 0.25c on both the suction and the pressure side of the airfoil.

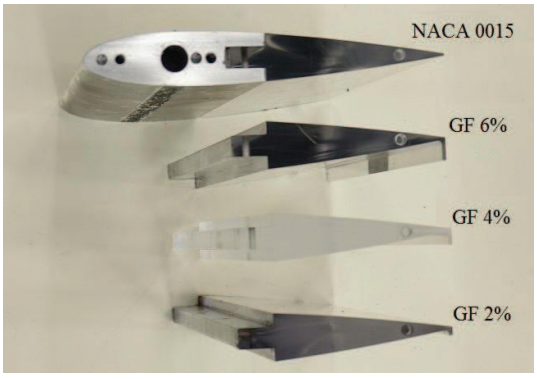

Fig 2: Gurney flap models

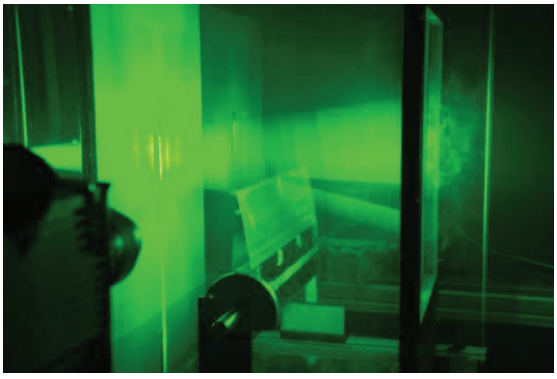

Fig 3: Photograph of the experimental set-up

To allow simultaneous PIV and acoustic measurements by microphones, two of the walls of the test sections are made out of Plexiglas and the other two of acosutically transparent Kevlar fabrics (Debrouwere, 2013). A slit in one of the Kevlar fabrics allows the laser light to illuminate the model (Figure 3).

A schematic for the Planar PIV measurements is shown in Figure 4. The illumination is provided by a Quantronix Darwin-duo dual cavity/single head pulsed Nd:YLF laser (λ = 527nm, pulse repetition rate=0.1-10kHz, 25 mJ per pulse at 1kHz). The laser beam is shaped into a sheet with a thickness of approximately 1 mm. Two Photron FASTCAM SA1 CMOS cameras (1024 × 1024 pixels, 12-bit, 20 μm pixel pitch, 5.4 kHz at full resolution) placed on either side of the test section are used for image acquisition. The sensor is cropped to 512 × 512 pixels to allow for an acquisition frequency of up to 8 kHz. The synchronization between the laser and camera is performed using the LaVision high speed controller and DAVIS 8.2 software. The flow is seeded with a SAFEX smoke generator (non-toxic water-glycol based fog) with particles of median size $d_p \approx 1\mu m$.

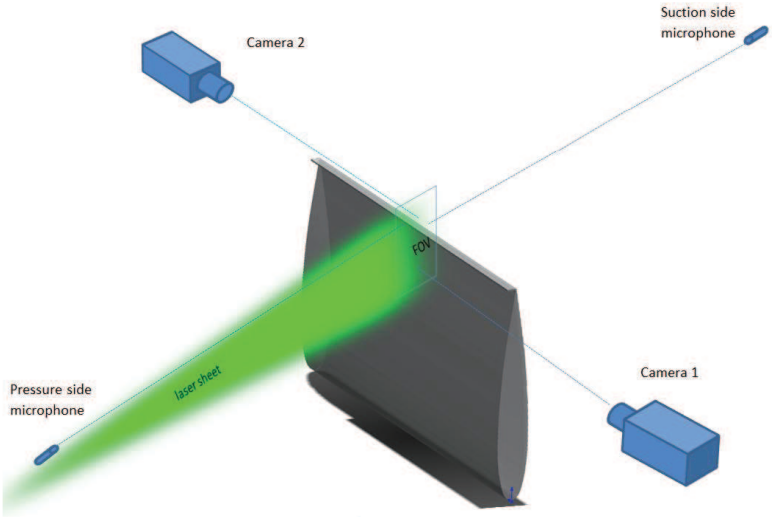

Fig 4: Schematic for simultaneous measurements

Simultaneous measurements of flow and acoustics are carried out for the GF 6% and GF 4% (Gurney flaps equal to 6% and 4% of the airfoil chord, respectively) using two cameras and four microphones (two each on suction and pressure side). The setup of the experiment is shown in Figure 5. The PIV recording parameters are reported in Table 1. An overlap of 1 cm in the field of view of the two cameras is kept to stitch the velocity fields obtained after processing of PIV images. The far-field acoustic fluctuations are measured using LinearX M51 microphones with

an acquisition frequency of 40kHz. In addition, statistical boundary layer measurements are carried out using a single camera and higher magnification on the suction side of the airfoil with parameters as shown in Table 1.

PIV parameters	Boundary layer measurement	Simultaneous flow/acoustic measurement
Field of View (FOV)	40 × 40 mm^2	50 × 50 mm^2 each camera
Optical magnification (M)	0.4	0.21
Focal length (f)	180 mm	105 mm in both cameras
Numerical aperture ($f_\#$)	5.6	2.8 in both cameras
PIV acquisition frequency (f_s)	50 Hz	5 kHz (U_∞ = 20 m/s), 8 kHz (U_∞ = 30 m/s)
Number of images (N)	2700	10,000
Digital image resolution	25 px/mm	10 px/mm
Interrogation window size	1.5 × 1.5 mm	0.625 × 0.625 mm
Interrogation window size in pixels	16 × 16 px	16 × 16 px

Table 1: PIV recording parameters for time resolved simultaneous and statistical boundary layer measurements

3. Results and discussions

Boundary layer

The mean streamwise velocity contour along with the boundary layer velocity profile are shown in Figure 6 for the 4% Gurney flap case at α =4° and freestream velocity u_∞= 30 m/s (GF4-AOA4-V30). The most relevant boundary layer properties such as boundary layer thickness δ_{95},

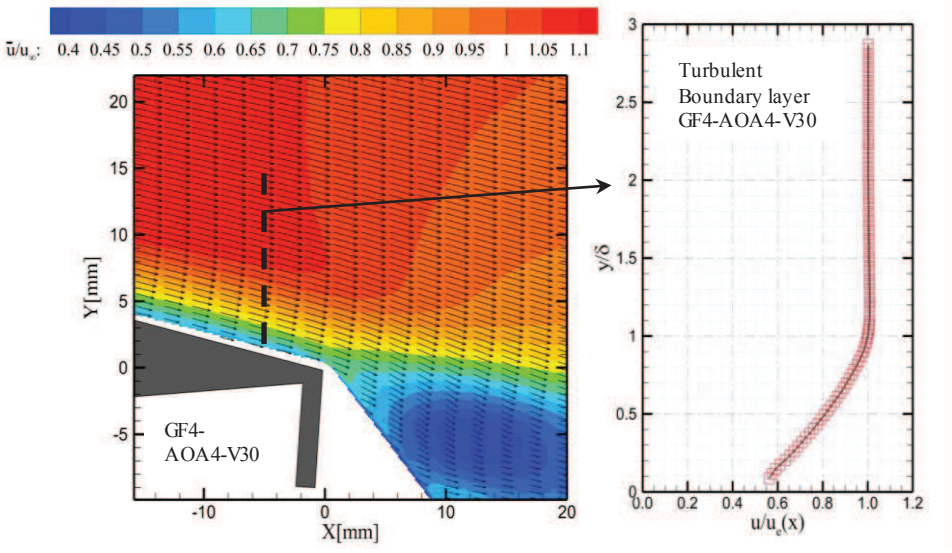

Boundary layer properties	
δ_{95}	6 mm
δ^*	0.94 mm
θ	0.62 mm
H	1.51

Fig 6: Boundary layer profile (at x/c=0.97) and statistical properties of the boundary layer for GF4-AOA4-V30 case

displacement thickness δ^* and momentum thickness θ are evaluated from the velocity profile at x/c = 0.97 (with a linear interpolation between 0 and first data point). The shape factor H=1.5 confirms the presence of a turbulent boundary layer (White, 2006).

Flow Statistics

The contours of the time-averaged velocity component $\bar{u}$, $\bar{v}$, along with root-mean-square of the fluctuations u'_{rms} ,v'_{rms} for the GF6-AOA8-V30 (Gurney flap size 6%, angle of attack 8° , free stream velocity 30 m/s) case are shown in Figure 7. From the mean streamwise contour plot of $\bar{u}$, three main features in the flow can be distinguished. First, a separation of the flow on the pressure side upstream of the Gurney flap, which creates a recirculation region. Second, the upper and the lower separating shear layers; finally, the main recirculation region downstream of the flap. Large fluctuations in the wake are seen clearly by v'_{rms} indicating coherent vortex shedding.

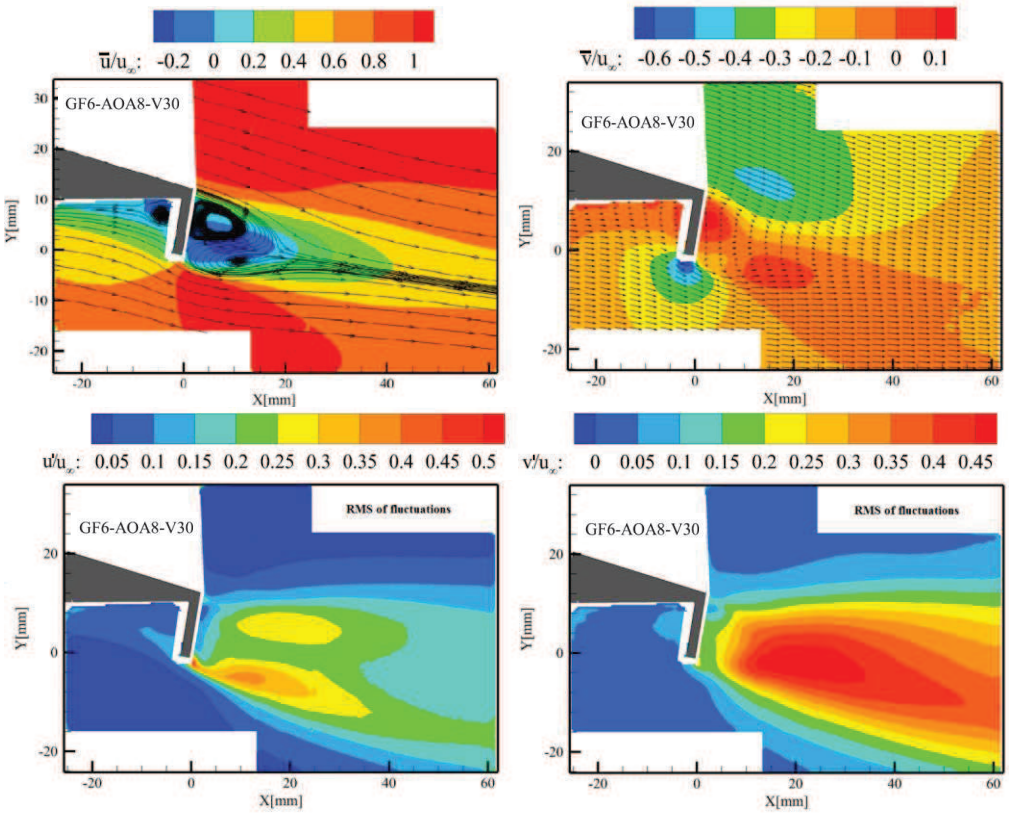

Fig 7: Flow statistics for GF6-AOA8-V30, $\bar{u}$ (top left) $\bar{v}$ (top right) u'_{rms} (bottom left) v'_{rms} (bottom right) at $Re_c = 4\times10^5$

Flow Dynamics

The contours of the instantaneous streamwise velocity component u show the flapping motion of the wake (Figure 8). The coherent shedding process is illustrated by the contours of instantaneous transverse velocity component v. The letters A and B indicate two flow structures that are convected downstream. The formation of a vortex street can be explained using Gerrad's (1966) widely accepted postulate for the mechanism of vortices shed behind bluff bodies (Jeffery *et al.* 2000). It occurs when two separating shear layers interact. The upper and lower boundary layers having opposite vorticity form two separating shear layers. When one of the shear layers rolls up and forms a vortex, the other shear layer cuts off the vorticity supply while shedding a vortex in the process.

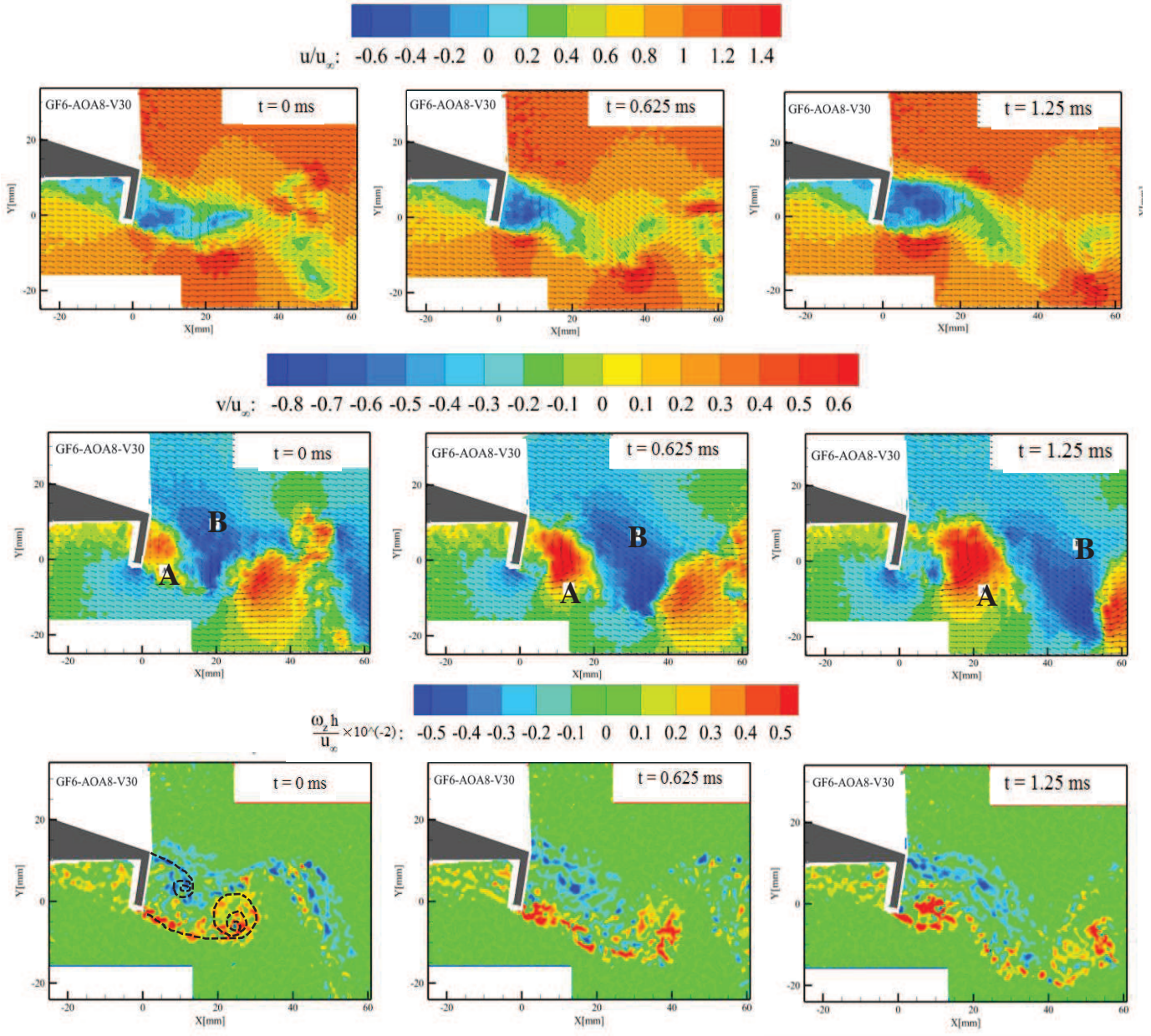

Fig 8: Flow statistics for GF6-AOA-V30, ū (top left) ū (top right) u'_{rms} (bottom left) v'_{rms} (bottom right) at Re_c =0.4 million

The instantaneous vorticity field is computed from the time-resolved velocity field as shown in Figure 8. The vorticity is computed with the three-point centered difference formula. The vortex roll up process can be seen clearly when vorticity is shed by both the upper and lower boundary layers. Positive vorticity (counterclockwise direction of the fluid) shed from the lower and negative vorticity shed by the upper boundary layer are seen interacting downstream of the flap leading to periodic vortex shedding.

Power spectral density of flow and acoustics

The PSD of v' at (X,Y) locations A, B and C is shown in Figure 9. A comparison with the PSD of the microphone (in dB) shows a tonal peak that corresponds to the coherent periodic shedding observed in the flow (f = 450 Hz, Strouhal number St = 0.18 based on flap height). This tonal peak was clearly audible during the experiments. Apart from the harmonics of the primary frequency, no prominent second peak is present in the acoustic and v' spectra.

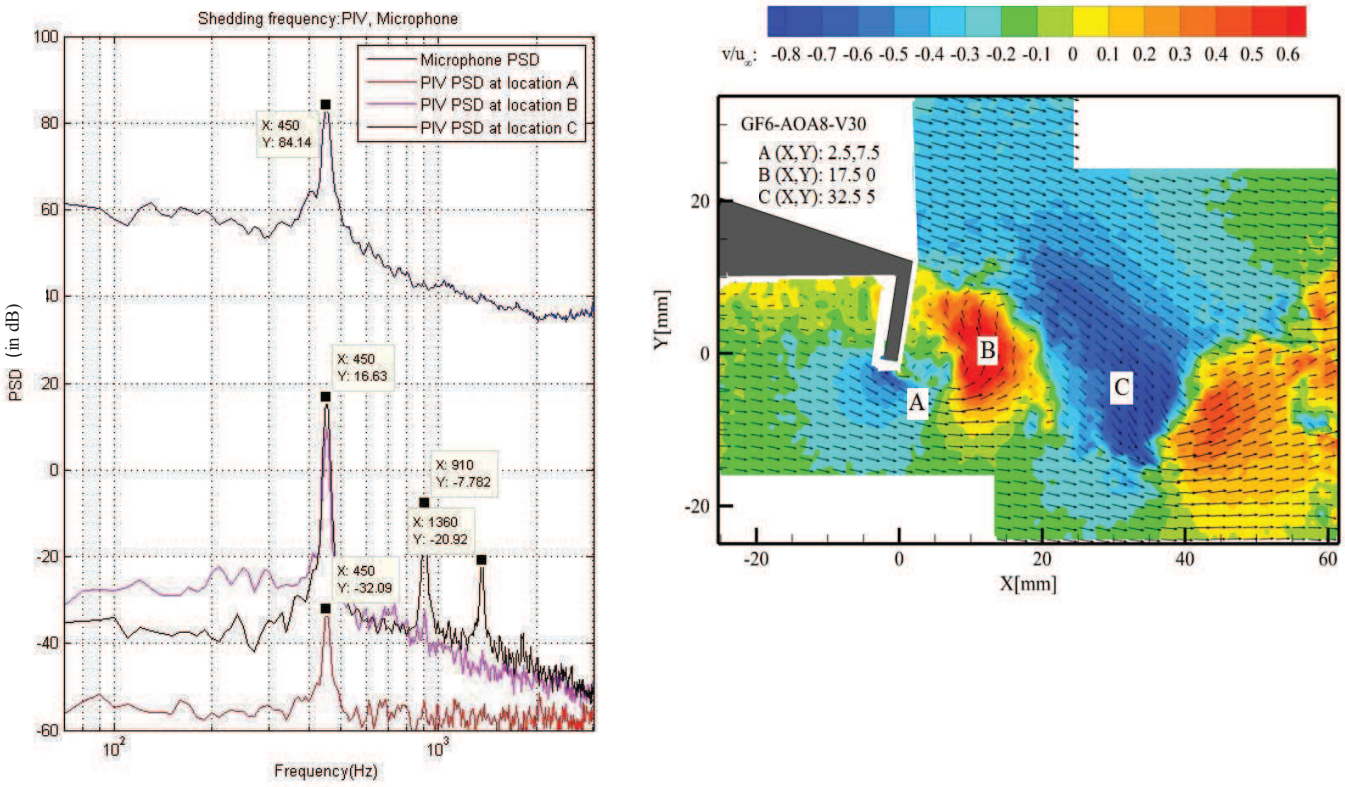

Fig 9: Frequency peak of PIV at location A, B and C compared with microphone for the GF6-AOA8-V30 case (left), location of points A, B and C, where the power spectra are extracted (right)

The absence of a secondary mode can be attributed to the presence of a turbulent boundary layer on both the suction and the pressure side. The secondary mode discussed by Troolin *et al.* (2006)

may be due to the presence of a laminar boundary layer instability especially on the pressure side, where the Gurney flap is located. The Strouhal number St = 0.18 is comparable to that obtained for a bluff body. For example, the flow around a cylinder yields St= 0.186 (Henning *et al.*, 2008), whereas a blunt trailing edge leads to tonal noise with St = 0.21 when the bluntness parameter $T/\delta^* \geq 3.3$ (Blake, 1986).

Causality correlation

The contour plots of the maximum value of the normalized cross correlation coefficient $R_{v'p'}$ are shown in Figure 10. Various cases are considered: Gurney flap height equal to 4% and 6% of the airfoil's chord (GF4 and GF6, respectively); angles of attach (AOA) of 4 and 8 degrees; free-stream velocity of 20 and 30 m/s (V20 and V30, respectively). $R_{v'p'}$ is close to zero in the upstream separation bubble indicating that the upstream separation bubble is not a source region for the tonal noise. The maximum value in the entire domain is $R_{v'p'} = 0.53$ for the GF6-AOA8-V30 case. Such high correlation suggests a direct relation between the velocity fluctuations downstream of the flap and the far-field noise.

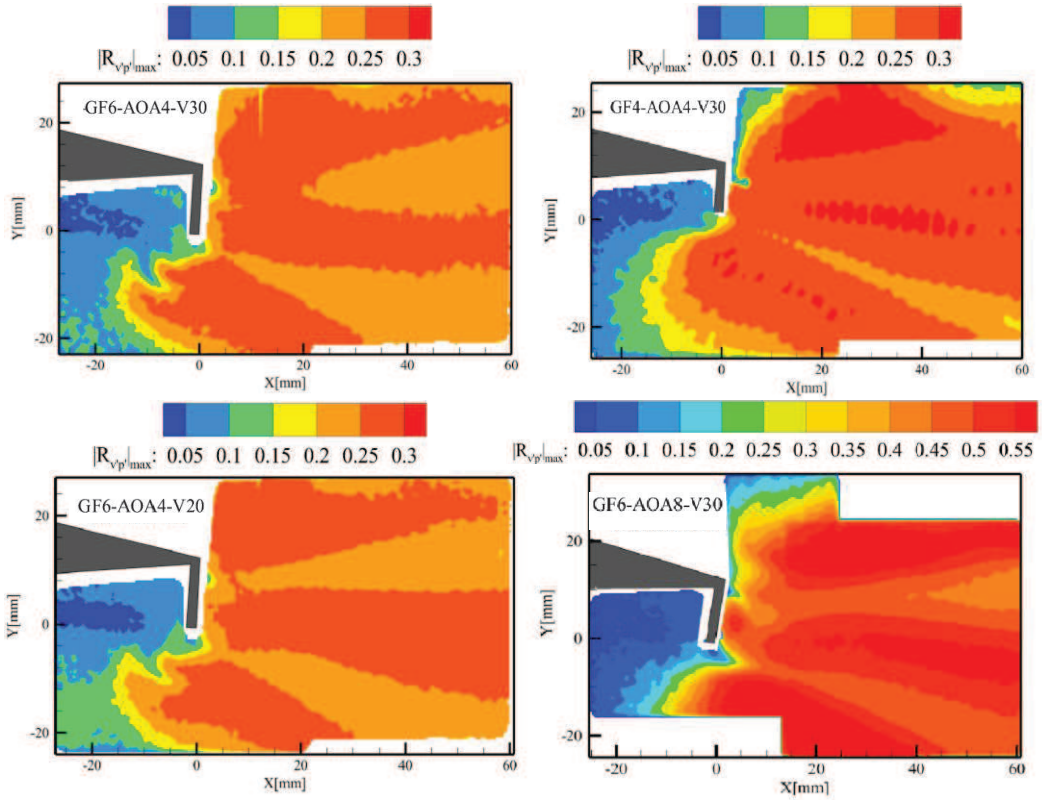

Fig 10: Maximum value of $R_{v'p'}$ for different cases (top left: reference case, top right: GF% decrease; top left, bottom left: Re decrease; top left, bottom right: α increase)

As recently pointed out by Henning *et al*. (2014), there can be some ambiguity on the location of the 'actual source' based on the maximum values of $R_{v'p'}$. One has to be careful while concluding that higher values of correlation represent the 'true source of sound' since there can be significant correlation in structures downstream of the upstream 'source of sound'. Therefore the high values of correlation in Figure 10 do not necessary mean they are the 'sources', but they can also be due to an upstream source and convected downstream. This is made clear when the correlation function as a function of τ shift, $R_{v'p'}(\tau)$, is calculated.

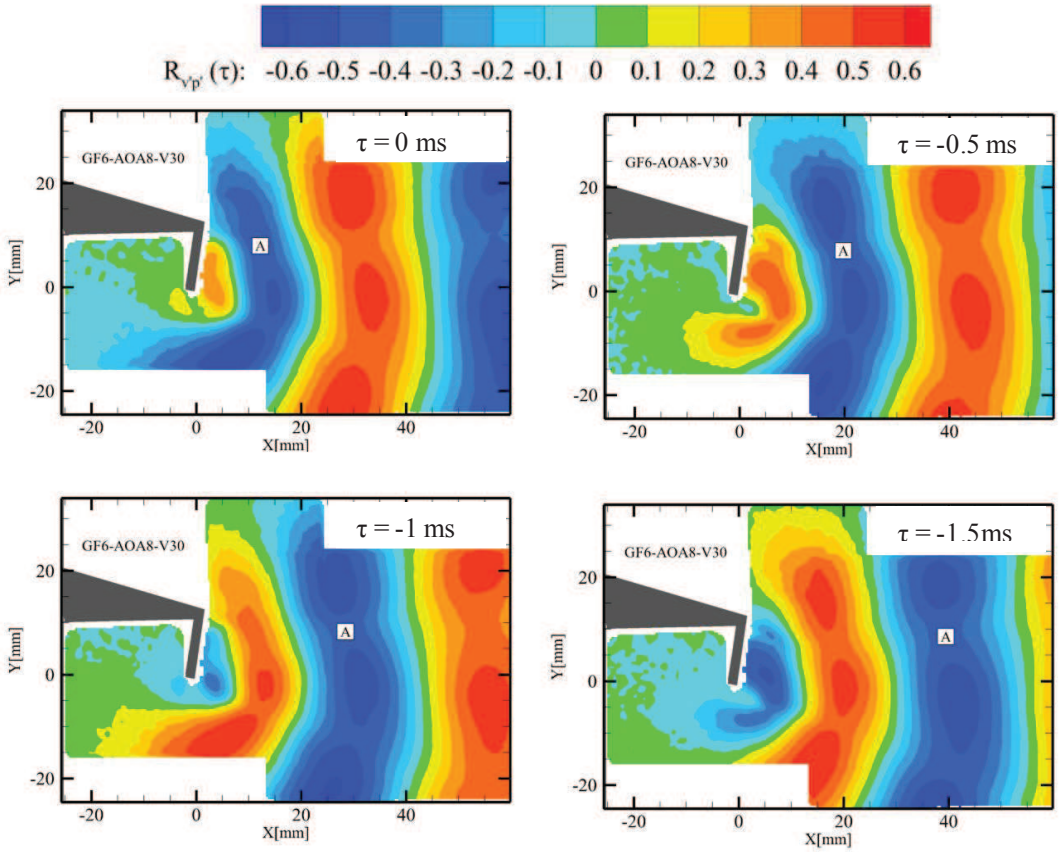

Fig 11: Contour plot of $R_{v'p'}(\tau)$ for different τ (GF6-AOA8-V30 case)

To calculate $R_{v'p'}$ as a function of τ shift, it is important to first take into account the propagation time of acoustic waves to the microphone. First τ_0, i.e. the point where zero lag between the two signals is present, is calculated using cross-correlation. The temporal shift corresponding to the maximum value of correlation between the two signals is taken as the 'starting point' of the two signals. This is done to take into account the propagation time as well as the delays due to errors in acquiring the measurements in a synchronized manner. The contour plot of $R_{v'p'}(\tau)$ (Figure 11) shows that shifting the acoustic pressure signal with respect to the v' fluctuations of the flow in the negative direction (τ decreasing from 0 to negative values) causes the correlation function to move in the downstream direction as indicated by letter A.

Thanks to the high temporal resolution of the measurements, Figure 11 shows that significant correlation is originated close to the flap, which is expected to be the main source of sound. At low Mach number flows, the dipole term caused by unsteady pressure (or lift) fluctuations is the main dominant source (Curle, 1955). The high values of correlation downstream of the flap are therefore due to the presence of an upstream source at the flap location. The flow features downstream of the flap are not strong sources of sound themselves: the high correlation with the far-field pressure fluctuations are merely due to the fact that the flow features originated at the Gurney flap are convected downstream.

Coherence

A drawback in correlating two signals in the time domain is that correlation does not allow distinguishing the different frequency contents of the signals. Thus, uncorrelated parts of the signals can reduce the overall magnitude of the correlation coefficient. On the other hand, coherence (or normalized cross-power spectral density) can be used to assess the frequency dependence of the signals.

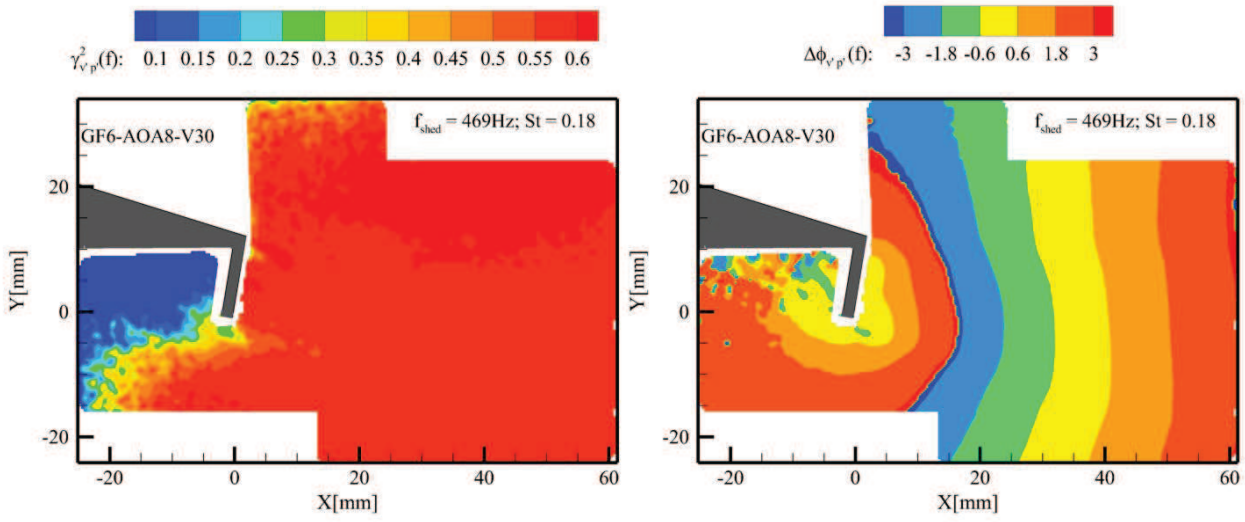

Fig 12: Contour plots of magnitude square coherence $\gamma^2{}_{v'p'}$ at shedding frequency (left) and the corresponding phase difference plot (right)

The magnitude square-coherence $\gamma^2{}_{\emptyset' p'}$ is defined by,

$$\gamma^2{}_{\emptyset\, p'}(f) = \frac{|G_{\emptyset\, p'}(f)|^2}{G_{\emptyset\,\emptyset}(f)\, G_{p'p'}(f)} \qquad (2)$$

where $G_{\emptyset p'}(f)$ is the cross spectral density between the near field fluctuations and the far field acoustic pressure fluctuations, and $G_{\emptyset\emptyset}(f)$, $G_{p'p'}(f)$ are the auto-spectral densities of the near and far-field fluctuations respectively.

$\gamma^2_{v'p'}$ (Figure 12) is calculated at the shedding frequency (450 Hz) for the GF6-AOA8-V30 case. The values obtained are slightly higher than the $R_{v'p'}$. The contour plot $\gamma^2_{v'p'}$ also shows very low values in the upstream recirculation region. Downstream of the Gurney flap, $\gamma^2_{v'p'}$ is almost equal everywhere in the domain. The phase difference between v' and p' fluctuations is calculated using the argument of $\gamma_{v'p'}$. The phase difference $\Delta\phi_{v'p'}$ obtained at the shedding frequency varies from π to - π (Figure 12). The convective velocity u_c of the large scale coherent flow structures is evaluated as the product between the wavelength from the phase difference plot and the shedding frequency (Pröbsting *et al*, 2016). The obtained wavelength is λ = 0.045 m, that yields u_c = 21.1 m/s or u_c/U_∞ = 0.7.

4. Conclusions

The flow dynamics and aeroacoustics of a NACA 0015 airfoil with a Gurney flap were investigated by simultaneous TR-PIV and microphone measurements. The measurements were conducted at Reynolds number between 2.5×10^5 and 4×10^5 based on the airfoil's chord. The boundary layer was tripped on both suction and pressure sides to ensure the presence of a turbulent boundary layer.

Coherent vortex shedding is produced downstream of the Gurney flap. The power spectral density of flow fluctuations as well as the acoustic spectra featured a clear peak at the frequency of vortex shedding. Contrary to the investigation of Troolin *et al*. (2006), no prominent secondary mode of shedding was found. This difference is attributed to the turbulent boundary layer in the present investigation. The tonal peaks were clearly audible and correspond to the vortex shedding frequency. TR-PIV resolves the ambiguity in the interpretation of the high values of correlation between velocity and pressure fluctuations. The high values of correlation far downstream of the Gurney flap are due to the presence of an upstream source (the flap) and are not sources of sound themselves. Thus, causality correlation using time-resolved data has good potential in identifying flow structures that are highly correlated with acoustic fluctuations in the far field. In the future, the technique can be applied to the relevant case of aircraft flap side edge noise, thereby making newer designs of flaps with lower-acoustic emissions possible.

References

International civil aviation organization (ICAO). (2013). environmental report.

Dobrzynski, W. (2010). Almost 40 Years of Airframe Noise Research: What Did We Achieve?, Journal of Aircraft, vol. 47, no. 2, pp. 353–367.

Jang, C. S., Ross, J. C., & Cummings, R. M. (1998). Numerical investigation of an airfoil with a Gurney flap. Aircraft Design, 1(2), 75.

Jeffrey, D., Zhang, X., & Hurst, D. W. (2000). Aerodynamics of Gurney flaps on a single-element high-lift wing. Journal of Aircraft, 37(2), 295-301.

Wang, J. J., Li, Y. C., & Choi, K. S. (2008). Gurney flap- Lift enhancement, mechanisms and applications. Progress in Aerospace Sciences, 44(1), 22-47.

Liebeck, R. H. (1978). Design of subsonic airfoils for high lift. Journal of aircraft, 15(9), 547-561.

Gerrard, J. H. (1966). The mechanics of the formation region of vortices behind bluff bodies. Journal of Fluid Mechanics, 25(02), 401-413.

Troolin, D. R., Longmire, E. K., & Lai, W. T. (2006). Time resolved PIV analysis of flow over a NACA 0015 airfoil with Gurney flap. Experiments in Fluids, 41(2), 241-254.

Troolin, D. R. (2009). A quantitative study of the lift-enhancing flow field generated by an airfoil with a Gurney flap. PhD thesis, University of Minnesota.

Siddon, T. E. (1973). Noise source diagnostics using causality correlations. AGARD CP, 131, 7-1.

Lee, H. K., & Ribner, H. S. (1972). Direct correlation of noise and flow of a jet. The Journal of the Acoustical Society of America, 52(5A), 1280-1290.

Curle, N. (1955). The influence of solid boundaries upon aerodynamic sound. In Proceedings of the Royal Society of London A: Mathematical, Physical and Engineering Sciences (Vol. 231, No. 1187, pp. 505-514). The Royal Society.

White, F. M., & Corfield, I. (2006). Viscous fluid flow (Vol. 3). New York: McGraw-Hill.

Panda, J., Seasholtz, R. G., & Elam, K. A. (2005). Investigation of noise sources in high-speed jets via correlation measurements. Journal of Fluid Mechanics, 537, 349-385.

Henning, A., Kaepernick, K., Ehrenfried, K., Koop, L., & Dillmann, A. (2008). Investigation of aeroacoustic noise generation by simultaneous particle image velocimetry and microphone measurements. Experiments in fluids, 45(6), 1073-1085.

Henning, A., Koop, L., & Ehrenfried, K. (2010). Simultaneous particle image velocimetry and microphone array measurements on a rod-airfoil configuration. AIAA journal, 48(10), 2263-2273.

Henning, A., Schröder, A., Krebs, I., & Agocs, J. (2010). Aeroacoustic investigations on a cold jet by means of simultaneous piv and microphone measurements. In Proceedings of the 15th international symposium on applications of laser techniques to fluid mechanics, Lisbon, Portugal.

Henning, A., Wrede, B., & Geisler, R. (2012). Aeroacoustic investigation of a high-lift device by means of synchronized PIV and microphone measurements. In Proceedings of the 16th international symposium on applications of laser techniques to fluid mechanics, Lisbon, Portugal.

Henning, A., Wrede, B., and Schröder, A. (2015). About the ambiguity of noise source localization based on the causality correlation technique In Proceedings of the 17th international symposium on applications of laser techniques to fluid mechanics, Lisbon, Portugal.

Blake, W. K. (1986). Mechanics of Flow-Induced Sound and Vibration, Academic Press.

Curle, N. (1955). The influence of solid boundaries upon aerodynamic sound. Proceedings of the Royal Society of London. Series A. Mathematical and Physical Sciences, 231(1187):505-514.

Pröbsting, S., Zamponi, M., Ronconi, S., Guan, Y., Morris, S. C., Scarano, F. (2016). Vortex shedding noise from a beveled trailing edge. International Journal of Aeroacoustics, accepted for publication.